



Poly(ADP-ribose) polymerase signaling of topoisomerase 1-dependent DNA damage in carcinoma cells

Giovanna D'Onofrio^a, Filomena Tramontano^a, Annalisa Susanna Dorio^b, Alessia Muzi^b, Valeria Maselli^a, Domenico Fulgione^a, Grazia Graziani^b, Maria Malanga^a, Piera Quesada^{a,*}

^a Department of Structural and Functional Biology, University Federico II of Naples, Italy

^b Department of Neuroscience, University of Rome Tor Vergata, Italy

ARTICLE INFO

Article history:

Received 30 July 2010

Received in revised form 17 September 2010

Accepted 20 September 2010

Keywords:

Topotecan (TPT)

PARP-1 and -2

PJ34 Inhibitor

p53

Carcinoma cells

ABSTRACT

A molecular approach to enhance the antitumour activity of topoisomerase 1 (TOP1) inhibitors relies on the use of chemical inhibitors of poly(ADP-ribose)polymerases (PARP). Poly(ADP-ribosyl)ation is involved in the regulation of many cellular processes such as DNA repair, cell cycle progression and cell death. Recent findings showed that poly(ADP-ribosyl)ated PARP-1 and PARP-2 counteract camptothecin action facilitating resealing of DNA strand breaks. Moreover, repair of DNA strand breaks induced by poisoned TOP1 is slower in the presence of PARP inhibitors, leading to increased toxicity.

In the present study we compared the effects of the camptothecin derivative topotecan (TPT), and the PARP inhibitor PJ34, in breast (MCF7) and cervix (HeLa) carcinoma cells either PARP-1 proficient or silenced, both BRCA1/2^{+/+} and p53^{+/+}.

HeLa and MCF7 cell lines gave similar results: (i) TPT-dependent cell growth inhibition and cell cycle perturbation were incremented by the presence of PJ34 and a 2 fold increase in toxicity was observed in PARP-1 stably silenced HeLa cells; (ii) higher levels of DNA strand breaks were found in cells subjected to TPT + PJ34 combined treatment; (iii) PARP-1 and -2 modification was evident in TPT-treated cells and was reduced by TPT + PJ34 combined treatment; (iv) concomitantly, a reduction of soluble/active TOP1 was observed. Furthermore, TPT-dependent induction of p53, p21 and apoptosis were found 24–72 h after treatment and were increased by PJ34 both in PARP-1 proficient and silenced cells. The characterization of such signaling network can be relevant to a strategy aimed at overcoming acquired chemoresistance to TOP1 inhibitors.

© 2010 Elsevier Inc. All rights reserved.

1. Introduction

The camptothecin derivative topotecan (TPT) is a DNA topoisomerase 1 (TOP1) inhibitor approved for the treatment of ovarian cancer, non small-cell lung cancer and under clinical investigation for a number of advanced solid tumours and haematological malignancies [1]. The drug reversibly abolishes the DNA religation activity of TOP1 generating single strand breaks (SSBs) to which the protein is covalently linked. Double strand breaks (DSBs) arise when replication forks collide with the SSBs and run off. Thus, TPT-induced DSBs are largely replication dependent or S phase specific [2,3].

Eukaryotes have two pathways for repairing DSBs: homologous recombination (HR) and non homologous end joining (NHEJ). The relative contribution of these two DSB repair pathways seems to differ depending on the cell cycle phase; HR acts mainly in the S

and G2 phases, whereas NHEJ acts mainly in the G1 phase [4,5]. For these reasons, TPT-induced replication-dependent DSBs are usually repaired by the HR pathway [6].

Poly(ADP-ribosyl)ation is a post-translational modification catalyzed by poly(ADP-ribose)polymerase-1 and -2 (PARP-1 and PARP-2) and is one of the earliest cellular responses to DNA damage. PARP-1 and PARP-2 belong to a family of enzymes that cleave β -NAD⁺ in nicotinamide and ADP-ribose to form long and branched (ADP-ribose) polymers (PAR) on glutamic acid residues within the primary sequence of PARP-1 and PARP-2 (automodification) and of other cellular proteins (heteromodification). This process causes chromatin decondensation around damage sites, recruitment of repair machineries, such as base excision repair complexes, and accelerates DNA damage repair [7,8]. In contrast, when DNA damage exceeds cell repair capacity PARP-1 undergoes cleavage by caspases into two fragments of 89 kDa and of 24 kDa, thereby avoiding futile cycling of PAR that would otherwise deplete the cell of β -NAD⁺ required for the onset of apoptosis [9]. Moreover, interaction of PAR with the p53 oncoprotein is able to modulate its transcriptional activity [10].

* Corresponding author. Tel.: +39 081 679165.

E-mail address: quesada@unina.it (P. Quesada).

PARP-1 also affects DSBs repair as indicated by the increased sensitivity of PARP-1-deficient cells to DSBs inducing agents, especially to camptothecin [2]. Furthermore, the molecular mechanisms underlying tumour chemosensitization to TOP1 poisons by PARP inhibitors have been in part clarified by recent findings showing that poly(ADP-ribosylated PARP-1 and PARP-2 counteract camptothecin action facilitating resealing of DNA strand breaks [11]. This occurs through noncovalent yet specific interaction of PAR with particular TOP1 sites which results in inhibition of DNA cleavage and stimulation of the religation reaction [12]. Another mechanism proposed to explain the potentiation of camptothecin cytotoxicity by PARP inhibitors, is via the inhibition of base excision repair system, of which PARP-1 and -2 are important components. This model is supported by the association of tyrosyl phosphodiesterase-1, which removes the TOP1 cleavable complex, with base excision repair components that interact with PARP-1 [13].

Indeed, PARP-1 inhibition enhances the cytotoxic effects of TPT [14]. The potential of PARP inhibitors to increase the efficacy of chemotherapy has led to the development of a wide range of specific inhibitors – quinazolinone derivatives – like NU1025 or PJ34 which display increased potency compared to the prototype 3-aminobenzamide (3-ABA) [15]. In this regard, we previously demonstrated a TPT-dependent PARP-1 activation in glioblastoma cells, while co-treatment with the PARP inhibitor NU1025 increased the TPT-dependent p53 up-regulation [16]. Moreover, we showed PJ34 chemo-potential of cisplatin in colon carcinoma cells [17].

It has been reported that PARP inhibitors would be particularly effective in BRCA1/2 mutated breast carcinoma cells [18]. In fact, PARP-1 and PARP-2 are required for the base excision repair pathway, whereas the BRCA proteins are critical for the HR pathway. Cells can survive when one repair system breaks down, but they start to die when both DNA repair mechanisms stop functioning.

Furthermore, a factor supposed to be involved in determining the sensitivity of cells to TOP1 inhibitors is p53. However, for breast cancer cells the p53 status was not found to be predictive of sensitivity to camptothecins [19].

On the basis of such evidences, we have investigated the role of PARP-1 in the DNA damage response to TOP1 inhibitors, in human BRCA1/2^{+/+} and p53^{+/+} mammary (MCF7) and cervix (HeLa) carcinoma cells treated with TPT as single agent or in association with a PARP inhibitor. Furthermore, TPT sensitivity of HeLa cells in which PARP-1 has been knocked down by RNA interference, has been compared to that of HeLa cells treated with the PARP inhibitor.

2. Materials and methods

2.1. Drugs, antibodies and chemicals

TPT was from Glaxo Smith-Kline (Verona, Italy) and PJ34 [N-(6-oxo-5,6-dihydrophenanthridin-2-yl)-(N,N-dimethylamino)acetamide] from Alexis Biochemicals (Vinci-Biochem, Firenze, Italy). The cocktail of protease inhibitors was from ROCHE-Diagnostic (Milano, Italy).

Nicotinamide adenine [adenylate-³²P] dinucleotide-[³²P]-NAD⁺ (1000 Ci/mmol, 10 mCi/ml) was supplied by GE Healthcare (Milano, Italy).

Propidium iodide (PI) and RNase were from Sigma–Aldrich (Milano, Italy).

PVDF (poly-vinylidene-fluoride) membrane was from MILLIPORE S.p.A. (Milano, Italy). Anti-PARP-1 mouse monoclonal antibody (F1–23) was from Alexis Biochemicals (Vinci-Biochem, Firenze, Italy) and anti-DNA TOP1 antibody from ABCAM, (Cambridge, UK). Anti-p53 (DO-1), anti-p21 (C-19), anti-BAX (P-19) and

anti-GAPDH (H-2) mouse monoclonal antibodies were from Santa-Cruz Biotechnology (DBA, Milano, Italy); anti-actin (A2066) mouse monoclonal antibody and goat anti-mouse and goat anti-rabbit IgG HRP-conjugated antibodies were from Sigma–Aldrich (Milano, Italy). Anti-γH2AX (ser139, 2577) rabbit antibody was from Cell Signaling (Invitrogen Milano, Italy).

All other chemicals were of the highest quality commercially available.

2.2. Cell cultures

Cervix (HeLa) and mammary (MCF7) carcinoma cells were maintained in Dulbecco's modified eagle's medium (DMEM) containing 10% (v/v) heat-inactivated foetal bovine serum (FBS), 100 U/ml penicillin, 100 mg/ml streptomycin, 5 mM L-glutamine and incubated at 37 °C in a humidified atmosphere, plus 5% CO₂.

Stably PARP-1 silenced HeLa cells (hereafter referred to as HeLa^{SIP-1}) or transfected with the pBabe vector carrying the puromycin resistance gene (hereafter referred to as HeLa^{Babe}) were obtained as previously described [20].

2.3. Cell growth inhibition

MCF7 and HeLa cells were seeded at 1 × 10⁵ cells; after 24 h, cell cultures were treated with graded concentrations of TPT and PJ34 and cell growth inhibition was assessed at different time points (24, 48, 72 h) using the 3-[4,5-dimethylthiazol-2-yl]-2,5-diphenyltetrazolium bromide (MTT) assay. All the experiments were performed in triplicate.

2.4. Cytofluorimetric analysis

Control and treated cells were detached by enzymatic treatment (trypsin/EDTA 0.02%), washed in PBS (w/o) Ca⁺⁺/Mg⁺⁺ pooled with floating cells and recovered by centrifugation at 1200 rpm for 15 min at 4 °C. Cells were fixed in 70% ethanol and stored at –20 °C until analysis. After washing in PBS (w/o) Ca⁺⁺/Mg⁺⁺, cells were stained in 2 ml of propidium iodide (PI) staining solution [50 μg/ml of PI, 1 mg/ml of RNase A in PBS (w/o) Ca⁺⁺/Mg⁺⁺, pH 7.4] overnight at 4 °C and DNA flow cytometry was performed in duplicate by a FACScan flow cytometer (Becton Dickinson Franklin Lakes, NJ, USA) coupled with a CICERO work station (Cytomation). Cell cycle analysis was performed by the ModFit LT software (Verity Software House Inc., Topsham, ME, USA). FL2 area versus FL2 width gating was done to exclude doublets from the G2/M region. For each sample 15,000 events were stored in list mode file.

2.5. Alkaline comet assay

Cells were suspended in PBS at a density of 10⁴ cells/ml and mixed with an equal volume of fresh low-melting agarose (LMA, 1% in PBS); 80 μl of agarose cell suspension was spread on normal-melting agarose (NMA, 1% in PBS) slides and covered with a cover-slip. Two slides were prepared per sample. After gelling for 5 min on an ice bed, the cover-slip was gently removed and another layer was added, cover-slipped and allowed to solidify for 5 min on ice before gently removing the cover-slip. The slides were then immersed in a freshly prepared ice-cold lysis solution (2.5 M NaCl, 0.1 M Na₂EDTA, 0.01 M Tris, 1% Triton X-100, 10% DMSO, pH 10) for 1 h. The slides were drained and placed in a horizontal electrophoresis tank filled with freshly prepared alkaline buffer (0.3 M NaOH, 1 mM Na₂EDTA, pH 13). Electrophoresis was carried out in this buffer for 20 min at 300 mA. Finally, the slides were gently washed twice in a neutralization buffer (Tris–HCl 0.4 M, pH 7.5) for 5 min to remove alkali and detergent, and stained with

50 μM DAPI (3 h). Images of a minimum of hundred cells from each sample were analysed on a fluorescence microscope (Nikon Instruments S.p.A. Firenze, Italy); overlapping figures were avoided from each slide. Quantitative assessment of DNA damage was performed using Comet Score 1.5 Image Analysis (TriTek Corporation, Sumerduck, VA, USA) software which computes the integrated intensity profile for each cell. DNA damage was measured as olive tail moment [(tail mean – head mean) \times % of DNA in the tail/100]. The results were analysed by Student's *t*-test and were considered statistically significant at $P < 0.008$.

2.6. Analysis of [^{32}P]-PAR synthesis

Following treatment with 10 μM TPT \pm 5 μM PJ34 of intact cell (5×10^6 cells/plate), [^{32}P]-PAR synthesis was determined by substituting the culture medium with 1 ml of 56 mM HEPES buffer pH 7.5, containing 28 mM KCl, 28 mM NaCl, 2 mM MgCl_2 , 0.01% digitonin, 0.1 mM PMSF, 1:25 dilution of a cocktail of protease inhibitors, 0.125 μM NAD^+ and 5 μCi [^{32}P]- NAD^+ (1000 Ci/mmol). After incubation at 37 $^\circ\text{C}$ for 30 min, cells were scraped off the plates, transferred to Eppendorf tubes and mixed with TCA at 20% (w:v) final concentration. After 15 min standing on ice, samples were collected by centrifugation at 1200 rpm for 15 min, washed twice with 5% TCA and three times with ethanol. [^{32}P]-PAR incorporated in the TCA-insoluble fraction was measured by Cerenkov counting using a LS8100 liquid scintillation spectrometer (Beckman Coulter S.p.A. Milano, Italy). Finally, TCA protein pellets were resuspended in Laemmli buffer; proteins were separated by 5–15% SDS-PAGE and after electroblotting on PVDF membrane, [^{32}P]-PAR acceptors were visualized by autoradiography. Immunodetection of specific proteins was accomplished on the same blots after autoradiography.

PJ34 efficiency as PARP inhibitor, was determined in an *in vitro* enzymatic activity assay using permeabilized cells: cell pellets were resuspended in 40 mM Tris-HCl pH 7.8, 0.6 mM EDTA, 30 mM MgCl_2 , 0.05% Triton X-100, 1 mM β -mercaptoethanol, 20% glycerol, 1 mM PMSF and a 1:25 dilution of the cocktail of protease inhibitors. To maximally stimulate PAR synthesis, DNA strand breaks were induced by sonication for 30 s at medium intensity; finally, samples were incubated at 30 $^\circ\text{C}$ for 1 h with 5 $\mu\text{Ci/ml}$ [^{32}P]- NAD^+ and 50 μM unlabeled β - NAD^+ , in the presence or absence of 5 μM PJ34.

Reactions were stopped by TCA addition (20% final concentration) and the samples were processed and analysed as described above.

2.7. Isolation of nuclear and post-nuclear fractions

To isolate sub-cellular fractions, cells were suspended in a buffer containing 30 mM Tris-HCl pH 7.5, 1.5 mM MgCl_2 , 10 mM KCl, 1% (v/v) Triton X-100, 20% glycerol, 2 mM PMSF and the protease inhibitors cocktail solution. After 30 min of incubation on ice, cellular suspensions were centrifuged at $960 \times g$ for 90 s at 4 $^\circ\text{C}$ and the nuclear fractions recovered in the pellet. The supernatant represents the post-nuclear fraction.

Nuclear fractions were resuspended in 20 mM HEPES pH 7.9, containing 20 mM KCl, 0.2 mM EDTA, 1.5 mM MgCl_2 , 25% glycerol and the protease inhibitors cocktail solution. Protein concentration was determined using the Bradford protein assay reagent (BIO-RAD, Milano, Italy) with bovine serum albumin as a standard.

2.8. Autoradiographic and immunological analyses

Aliquots of 120 μg of cellular proteins were separated by SDS-PAGE (5–15% gradient gels) and transferred onto a PVDF membrane using an electroblotting apparatus (BIO-RAD). The membrane was subjected to autoradiographic analysis by the PhosphorImager (BIO-RAD) and/or to immunodetection after blocking with 5% non-

fat milk in TBST 1 h, with anti-PARP-1 (F1–23; diluted 1:5000), anti-TOP1 (Sc1-70; diluted 1:2500), anti-p53 (DO-1; diluted 1:5000), anti-p21 (C-19; diluted 1:1000), anti-Bax (P-19; diluted 1:500), anti-GAPDH (H2; diluted 1:5000), anti- γH2AX (2577; diluted 1:1000) and anti-actin (A2066; diluted 1:1000).

As secondary antibodies goat-anti-mouse or goat-anti-rabbit IgG HRP-conjugate (diluted 1:10,000–1:20,000) in 3% (w/v) non-fat milk in TBST were used. Peroxidase activity was detected using the ECL Advance Western blotting kit of GE Healthcare (Milano, Italy) and quantified using the Chemiluminescent detection system GS710 (BIO-RAD) and the Quantity One software: the arbitrary densitometric units were normalised on those of the GAPDH loading control.

3. Results

3.1. Effect of PJ34 on TPT-induced growth inhibition in human carcinoma cells

In preliminary experiments human cervical (HeLa) and mammary (MCF7) carcinoma cell lines showed comparable TPT-dependent growth inhibition, as measured by the MTT assay (data not shown). Furthermore, PARP-1 silencing by stable shRNA expression in HeLa cells (HeLa^{SIP-1}) rendered these cells more sensitive to the cytotoxic effects of the drug. In particular, while in a 72 h assay, 10 μM TPT for 1 h exerted mainly cytostatic effects in control cells (HeLa^{Babe}), the same treatment caused 45% (± 5) of PARP-1 silenced cells (HeLa^{SIP-1}) to die. In the presence of 5 μM PJ34 30% (± 6) of PARP-1 proficient and 60% (± 9) of PARP-1 deficient cells underwent cell death (data not shown).

To gain insight into the mechanism of enhanced TPT toxicity as a consequence of alteration of the cellular poly(ADP-ribosylation) status, we analysed cell cycle distribution at different recovery times after 1 h exposure to increasing concentrations of TPT, in the presence or absence of a functional PARP-1 (i.e., PARP-1 wild type HeLa or MCF7 cells versus HeLa^{SIP-1} cells). In another set of experiments, the PARP inhibitor PJ34 was used in combination with TPT, at a fixed concentration of 5 μM , maintained in the culture medium all over the recovery time. As shown in Fig. 1, as early as 24 h after treatment, graded concentrations of TPT induced a progressive increase of cell accumulation in the G2/M phase starting from 0.2 μM up to 1.25 μM . Higher TPT concentrations, instead, promptly arrested the cells in S phase.

The addition of the PARP inhibitor PJ34 to TPT concentrations $< 1.25 \mu\text{M}$ significantly increased G2/M cell accumulation, whereas when combined with $\geq 1.25 \mu\text{M}$ TPT concentrations, PJ34 induced S phase cell accumulation. As also shown in Fig. 1 cell cycle kinetics was unaffected by treatment of HeLa^{Babe} cells with PJ34 used as single agent.

HeLa^{SIP-1} cells treated with TPT concentrations comprised between 0.2 and 0.4 μM underwent a more pronounced increase of G2/M cell accumulation with respect to HeLa^{Babe} cells exposed to the same concentrations of the TOP1 poison. Interestingly, 0.4 μM TPT caused in HeLa^{SIP-1} cells effects comparable to those observed in HeLa^{Babe} cells treated with 0.4 μM TPT plus the PARP inhibitor. However, PARP-1 silenced cells retained sensitivity to PJ34 and the combination 1.25 μM TPT + PJ34 caused S phase accumulation at a higher extent in HeLa^{SIP-1} than in HeLa^{Babe} cells (Fig. 1).

Cytofluorimetric analyses at a longer recovery time (i.e., 72 h after treatment), revealed that alterations of the poly(ADP-ribosylation) system caused TPT to be cytotoxic at a concentration (1.25 μM) that was primarily cytostatic in control cells, as indicated by the appearance of a sub-diploid peak (apoptotic cells) both in PARP-1 silenced (HeLa^{SIP-1}) and PJ34-treated PARP-1 wild type cells (HeLa^{Babe}) (Fig. 2). In this regard, the lack of

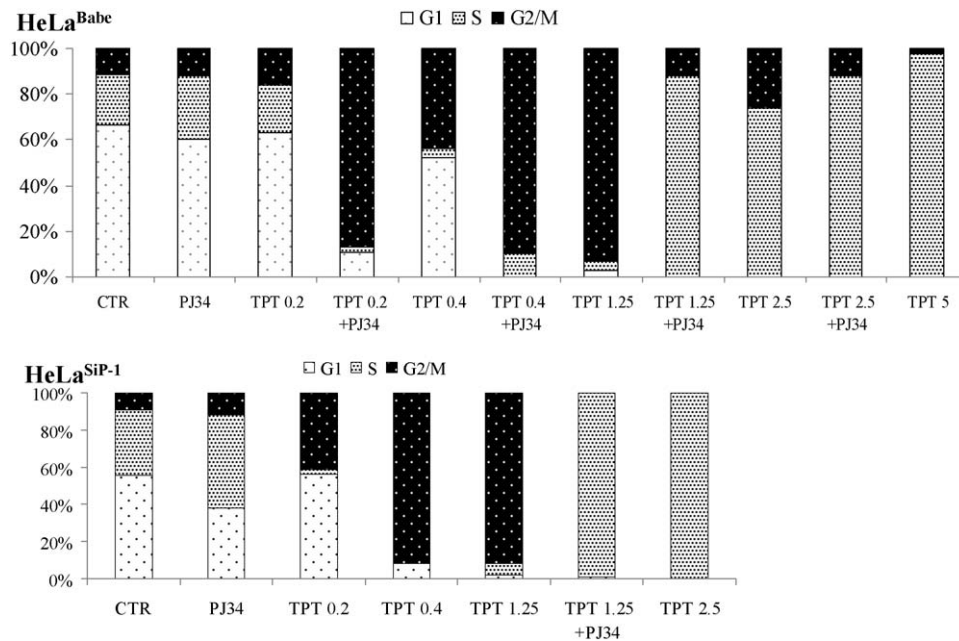


Fig. 1. Cell cycle analysis of HeLa^{Babe} and HeLa^{SiP-1} cells treated with TPT and PJ34 as single agents or in combination. Babe and SiP-1 cells were treated for 1 h with TPT (0.2–0.4–1.25–2.5–5 μ M) in combination or not with PJ34 (5 μ M) and left to recover for 24 h in fresh medium in the presence or absence of PJ34. The results are expressed as percentages of cells in the G1, S and G2/M phase of the cell cycle. Data refer to one out of three experiments giving similar results.

PARP-1 appeared to be more effective than PARP activity inhibition as the fraction of apoptotic cells was 62% in TPT-treated HeLa^{SiP-1} versus 38% in HeLa^{Babe}, subjected to a combined TPT + PJ34 treatment (Fig. 2).

3.2. Analysis of TPT and/or PJ34 dependent DNA damage in carcinoma cells

By alkaline comet assay, we analysed the level of both SSBs and DSBs [21] induced by 10 μ M TPT \pm PJ34 treatments. Fig. 3(A) shows that the olive tail moment determined for both HeLa (Babe and SiP-1) and MCF7 cells 24 h after 1 h treatment with TPT was increased in the cells left to recover in the presence of PJ34. The definition of a DSBs level was obtained by looking at the H2AX phosphorylation in

isolated nuclei from Babe and SiP-1 cells. Fig. 3(B) shows that 72 h after 1 h treatment TPT induced a higher level of histone phosphorylation in HeLa^{SiP-1} than in HeLa^{Babe} cells. H2AX phosphorylation was further incremented by PJ34 addition in both PARP-1 proficient and silenced cells.

3.3. Analysis of PAR synthesis in carcinoma cells after treatment with TPT \pm PJ34

First, PJ34 efficacy as a PARP inhibitor at the concentration used in this study was assessed in an in vitro enzyme activity assay by incubating permeabilized and sonicated HeLa cells with exogenous 50 μ M [³²P]-NAD⁺ in the presence or absence of 5 μ M PJ34. Sonication was performed to induce DNA strand breaks and

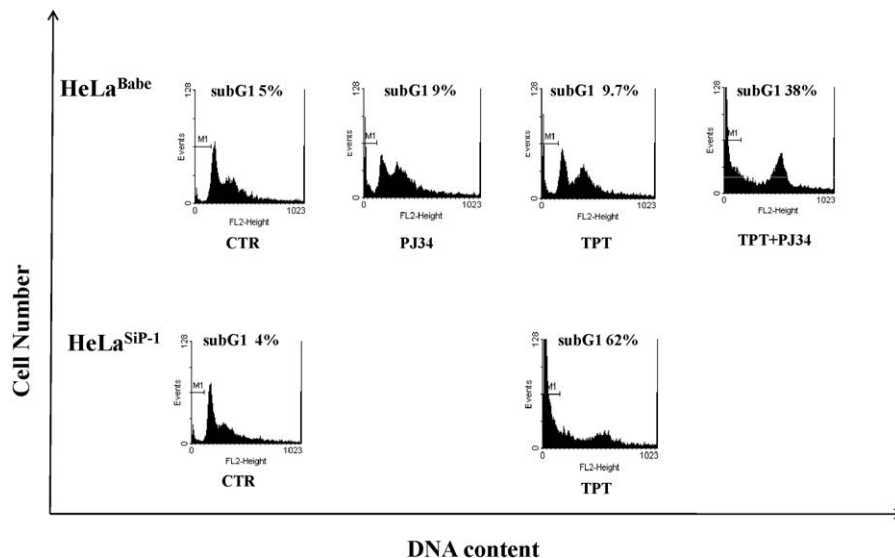


Fig. 2. Cell death analysis of HeLa cells subjected to TPT and PJ34 single and combined treatments. Babe and SiP-1 cells were treated for 1 h with 1.25 μ M TPT in combination or not with 5 μ M PJ34 and left to recover for 72 h in fresh medium in the presence or absence of PJ34. Flow cytometric determination of DNA content after PI staining is shown. The percentage of cells in the sub-diploid (subG1) peak is indicated. Data refer to one out of three experiments giving similar results.

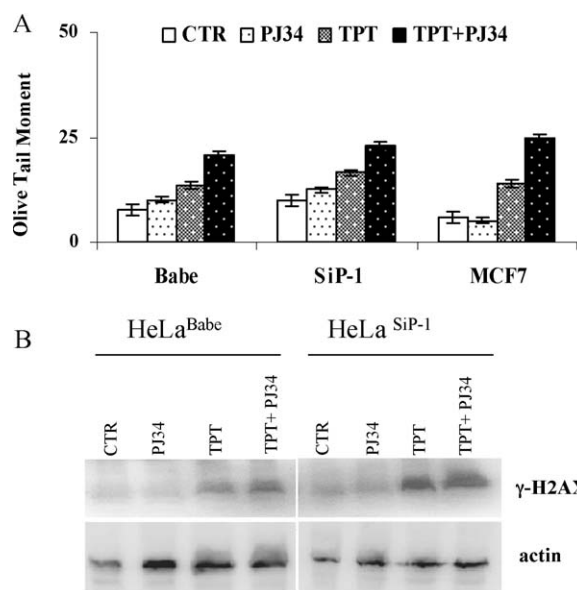


Fig. 3. DNA damage in HeLa^{Babe}, HeLa^{SiP-1} and MCF7 cells subjected to TPT ± PJ34 treatment. (A) Hundred cells 24 h after 1 h treatment with 10 μM TPT ± 5 μM PJ34 were analysed by alkaline comet assay on a fluorescence microscope (Nikon) and quantitative assessment of DNA damage was performed using Comet Score. The olive tail moment is reported as a mean of three different experiments ± S.E. (B) Western blot analysis of γH2AX levels in HeLa^{Babe} and HeLa^{SiP-1} cell nuclei treated 1 h with 10 μM TPT and allowed to recover in fresh medium in the presence or absence of 5 μM PJ34 for 72 h. Actin was used as loading control.

thus maximally stimulate endogenous PARP activities. PAR synthesis on protein acceptors was analysed by SDS-PAGE followed by electroblotting onto PVDF membrane and autoradiography. As shown in Fig. 4(A), a high amount of protein-bound PAR was produced in HeLa cells and such an activity was completely inhibited by 5 μM PJ34. Although a wide range of modified proteins could be visualized, the main PAR acceptor was most likely PARP-1 as suggested by the strong radioactivity signal at the top of the gel and by the concomitant reduction of the PARP-1 immunoreactive band in the sample incubated with β-NAD⁺ alone compared to that incubated with β-NAD⁺ and PJ34 (Fig. 4(B)). Such a difference is explained by a band depletion due to the automodification-related electrophoretic mobility shift of a fraction of heavily poly(ADP-ribosylated) PARP-1. After quantification of immunoreactive bands by scanning densitometry and normalization of PARP-1 to GAPDH content it could be estimated that about 50% of PARP-1 underwent automodification.

The same kind of analysis carried out in HeLa^{SiP-1} cells, revealed a strongly reduced ADP-ribosylation capacity of these cells as a consequence of PARP-1 silencing (Fig. 4(A)): on the autoradiography only a light smear at the top of the gel could be visualized. As no PARP-1 could be detected in these cells by Western blotting (Fig. 4(B)) the modest ADP-ribosylation activity detected by the *in vitro* assay may be due to PARP-2 and/or other PARP.

Then, we used a different experimental setting to determine whether or not TPT could induce PARP(s) activation in intact cells. To this purpose, growing MCF7 cells were first exposed to the drugs and then PAR synthesis was measured *in situ* by incubation in the presence of 0.01% digitonin and 0.125 μM [³²P]-NAD⁺. By autoradiography (Fig. 5(A)) we observed a main signal slightly up to PARP-1 molecular weight (113 kDa), indicating that DNA damage induced by TPT caused PARP-1 activation and automodification that was apparent already after 1 h treatment and further increased in the following 24 h recovery time. Such a trend was confirmed by scanning densitometry and normalization of

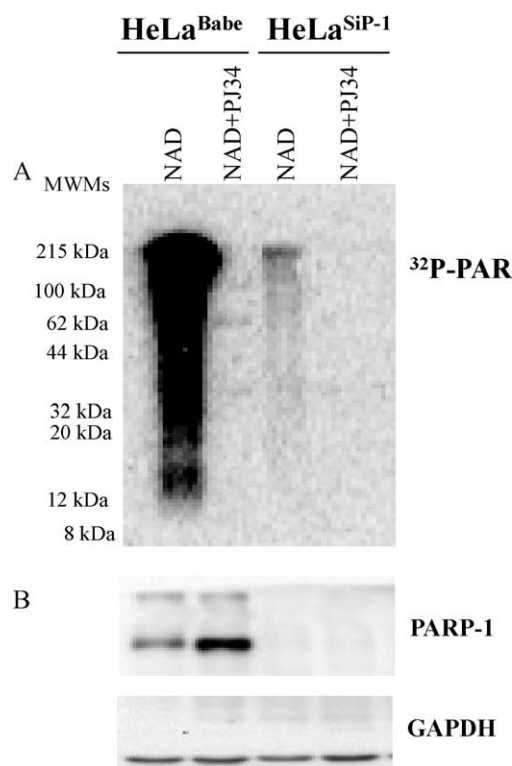


Fig. 4. PJ34-dependent inhibition of PAR synthesis in HeLa^{Babe} and HeLa^{SiP-1} cells. Cells were resuspended in lysis buffer, sonicated and incubated with 50 μM [³²P]-NAD⁺ ± 5 μM PJ34 as described in Section 2. (A) Autoradiographic analysis of whole cell protein after SDS-PAGE and electroblot on PVDF. (B) Immunodetection of PARP-1 and GAPDH on the blot shown in (A).

data from autoradiography (Fig. 5(A)) to those relative to PARP-1 immunoreactive band (Fig. 5(B)). Minor autoradiographic bands were evident in the 90–50 kDa MWs range (Fig. 5(A)) indicating other PAR acceptors, possibly including other PARP. PARP-2 was detectable in this region as a 62 kDa protein band; a modification-related electrophoretic mobility shift could explain the lack of correspondence between the autoradiographic signal (Fig. 5(A)) and the PARP-2 immunoreactive band (Fig. 5(B)).

The autoradiographic signals were drastically reduced (up to 75% reduction) in cells co-treated with TPT and the PARP inhibitor with respect to cells treated with TPT as single agent.

Similar results were obtained in HeLa^{Babe} cells, while a [³²P]-PAR signal was undetectable in HeLa^{SiP-1} (data not shown).

3.4. Immunological analysis of PARP-1, TOP1, p53, p21 level in TPT ± PJ34 treated cells

By Western blotting we analysed changes in the endogenous levels of PARP-1, TOP1 and p53 in HeLa and MCF7 cells at different times (24, 48 and 72 h) after treatment with TPT ± PJ34.

Fig. 6 shows a comparable amount of PARP-1 in MCF7 cell samples at all time points, whereas the amount of soluble/active TOP1 was lowered (~50%) till 72 h after treatment with TPT alone or in combination with PJ34. Conversely, an up-regulation of p53 endogenous levels was evident until 72 h after treatment with TPT ± PJ34. Furthermore, the p53-dependent p21 induction was evidenced starting from 24 h after TPT treatment.

Fig. 7 shows that the amount of soluble/active TOP1 was drastically lowered also in HeLa cells (up to 70–80% reduction both in PARP-1 proficient and silenced cells) as a consequence of the treatments. Interestingly, such a decrease was sustained till 72 h after 1 h treatment.

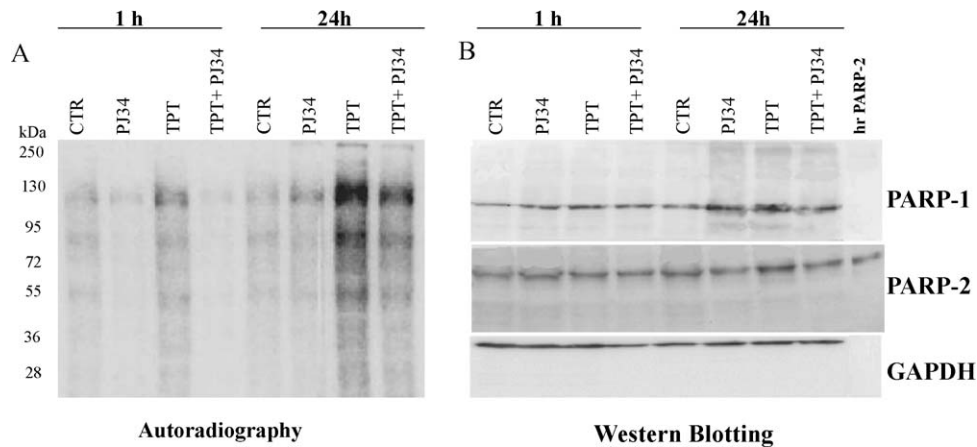


Fig. 5. TPT-dependent PARP activation in MCF7 cells. Following treatment with 10 μ M TPT \pm PJ34 and recovery for 24 h in fresh medium in the presence or absence of 5 μ M PJ34, cells were incubated with 0.125 μ M [32 P]-NAD $^{+}$, as described in Section 2. (A) Autoradiographic analysis of whole cell protein after SDS-PAGE and electroblot on PVDF. (B) Immunodetection of PARP-1, PARP-2 and GAPDH on the blot shown in (A). Fifty ng of human recombinant PARP-2 (hrPARP-2) was also loaded as a standard.

Again, we observed a TPT-dependent p53 up-regulation in both PARP-1 proficient and silenced cells, which appeared further increased by the use of PARP inhibitor (Fig. 7).

By densitometric scanning of immunoreactive bands we quantified the changes in p53 levels at different times after single and combined treatments. As shown in Fig. 8, the p53 level was 2–4 fold increased in HeLa^{Babe} cells 72 h after 1 h TPT \pm PJ34 treatment. In HeLa^{SiP-1} cells a 10 fold increase was induced by TPT alone and this value increased (13 fold) in the presence of PJ34 during the recovery time.

Finally, 72 h after TPT treatment we analysed the expression of apoptotic markers. Fig. 9 shows in HeLa^{Babe} cells the caspase-dependent PARP-1 cleavage. In MCF7 cells, instead, the PARP-1 apoptotic fragment was hardly detectable but we observed the p53-dependent expression of BAX. Interestingly, we found that PJ34 was able to enhance both such apoptotic signals.

4. Discussion

The evaluation of PARP inhibitors as chemosensitizers is based on evidences linking PARP-1 and recently PARP-2, to the cellular DNA damage response [13]. This has led to the development of a multitude of potent inhibitors with various bioavailability and pharmacokinetic characteristics whose efficacy in the treatment of cancer in vivo has been evaluated in animal models [14,22]; several PARP inhibitors are currently under investigation in clinical trials [15,23]. However, a clear understanding of the mechanism(s)

whereby PARP inhibitors potentiate the activity of antineoplastic agents is still lacking. Moreover, isoform specific PARP inhibitors are still missing while it is known that PARP-2 accounts for 10–20% of the total PARP activity in response to DNA damage [24 and references therein].

In our studies we used the hydrophilic PARP inhibitor PJ34 that has been recently reported to synergize with cisplatin in triple-negative breast cancer cells [25], in combination with the DNA TOP1 inhibitor, TPT. For our experiments we performed 1 h treatment with up to 10 μ M TPT that was already reported to be sufficient for trapping TOP1 in MCF7 cells [26]. PJ34 was used at a concentration (5 μ M) that was capable of inhibiting PARP activity but devoid of cytotoxic effects we found that TPT toxicity was higher when PAR synthesis was strongly reduced by either PARP-1 silencing (HeLa^{SiP-1} cells) or PJ34 administration (both in HeLa and MCF7 cells).

MCF7 and HeLa cells, according with their comparable PARP-1^{+/+} + BRCA1/2^{+/+} and p53^{+/+} status showed the same sensitivity to TPT, which determined a cell cycle arrest until 72 h after treatment. However, in combination with PJ34, TPT was cytotoxic even at a very low concentration (1.25 μ M). Accordingly, 1.25 μ M TPT alone was cytotoxic in PARP-1 silenced cells (HeLa^{SiP-1}). Nevertheless, the PARP inhibitor further increased the sensitivity of SiP-1 cells with respect to PARP-1 proficient cells treated with the drug combination, suggesting a PARP-2 involvement in the signaling of TPT-dependent DNA damage.

Consistently with the idea that poly(ADP-ribosyl)ation plays a role in the response to TPT-induced DNA damage, we found

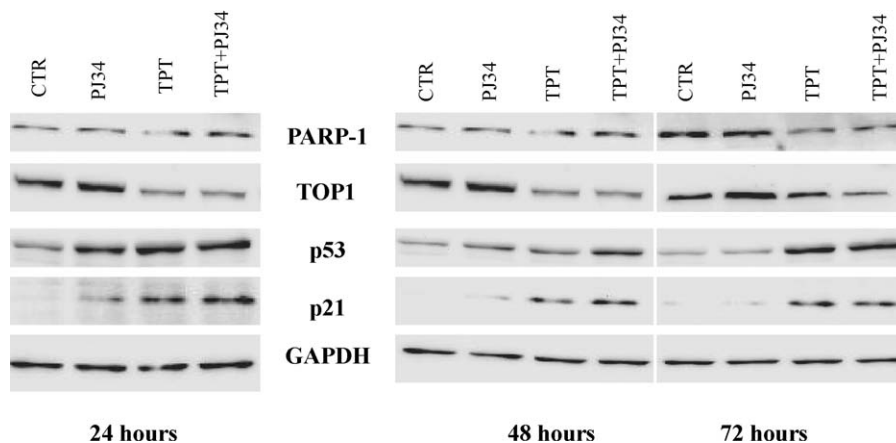


Fig. 6. Western blot analysis of PARP-1, TOP1, p53 and p21 in MCF7 cells. Cells were treated with 10 μ M TPT for 1 h and allowed to recover in fresh medium in the presence or absence of 5 μ M PJ34 for the indicated times. GAPDH was used as loading control.

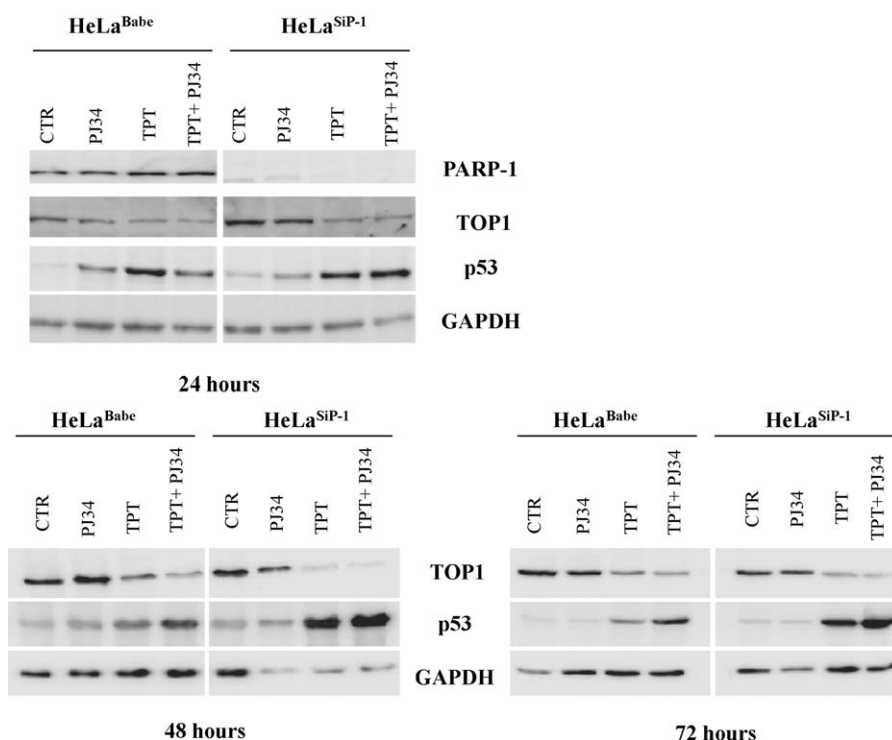


Fig. 7. Western blot analysis of PARP-1, TOP1, p53 and p21 in HeLa^{Babe} and HeLa^{SiP-1} cells. Cells were treated with 10 μ M TPT for 1 h and allowed to recover in fresh medium in the presence or absence of 5 μ M PJ34 for the indicated times. GAPDH was used as loading control.

increased PAR synthesis following cell exposure to 10 μ M TPT. The PARP inhibitor PJ34 prevented PARP activity and concomitantly caused intensification of cell cycle perturbations and increased DNA damage.

In particular, we observed distinct cell cycle perturbation effects depending on the concentration of the TOP1 inhibitor and on the association with the PARP inhibitor: in the low TPT dose range, PJ34 in combination with 0.2–0.4 μ M TPT caused more cells to be arrested in the G2/M phase, whereas combined with 1.25 μ M TPT it arrested at the S phase cells that escaped TPT action. Furthermore, the G2/M block induced by 0.4 μ M TPT in PARP-1 wild type cells was magnified in PARP-1 silenced HeLa cells. These evidences agree with the concept that after 1 h pulse (whatever the dose) of TPT not all the cells are prevented from entry in mitosis and then G2 cell lineages could survive TPT-mediated cytotoxicity [27]. Therefore, accumulation at the G2/M phase of tumour cells that escaped TPT action, provoked by PARP inhibition or by PARP-1

silencing, can be seen as a mechanism to overcome resistance to camptothecin derivatives. Interestingly, in PARP-1 silenced HeLa cells PJ34 increased the TPT S phase arrest as a further indication of PARP-2 implication.

Consistently, the TPT-dependent DNA damage level was increased by co-treatment with PJ34 both in PARP-1 proficient and PARP-1 silenced cells 24 h after treatment. In nuclei of such cells, differences in γ H2AX levels deriving from TPT \pm PJ34, also support PARP-1 and -2 stimulation of TPT-dependent DSBs repair.

Moreover, we found a sustained PAR synthesis from 1 to 24 h after treatment and most of the newly synthesized polymer was linked to PARP-1 itself. Two other PAR acceptors in the 55–95 kDa MW's range appeared to be TPT- and PJ34-dependent. Accordingly with the magnified effects of TPT + PJ34 treatment in PARP-1 silenced cells the PARP-2 modification could represent the mechanism of its participation in DSBs signaling and HR repair [24].

Indeed, these evidences suggest that the lack of PAR synthesis, by interfering with the repair of TOP1-induced DNA damage, causes DNA strand breaks accumulation and further delays cell cycle progression. Moreover, we found that TPT-treated cells entered the apoptotic program as a consequence of PARP-1 silencing and/or PARP inhibition.

The last set of results was based on mechanistic investigations addressed to show the long-term response to TPT action: after 1 h TPT pulse TOP1 soluble/active fraction was drastically reduced for at least 3 cell duplication cycles and p53/p21 levels increased within the same time frame. Such an up-regulation was even higher in cells lacking PARP-1 and further increased by TPT + PJ34 treatment, supporting again the involvement of PARP-2 in the signaling of TPT-dependent DNA damage.

These results are in agreement with those previously reported in the same cells treated with the methylating agent temozolomide in combination with the PARP inhibitor GPI 15427, suggesting the involvement of PARP-2 (or other PARP) in the repair of DNA damage provoked by temozolomide [20].

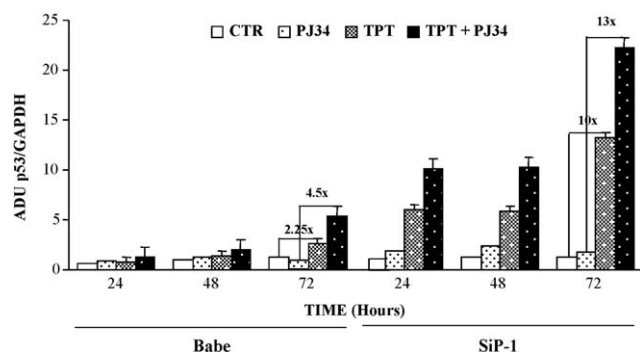


Fig. 8. Densitometric analysis of p53 levels in HeLa cell samples. After immunodetection on Western blots, band intensities were quantified by scanning densitometry. Data, expressed as arbitrary densitometric units (ADU), were normalized to the internal control GAPDH. Shown are the mean of three different experiments \pm S.E.

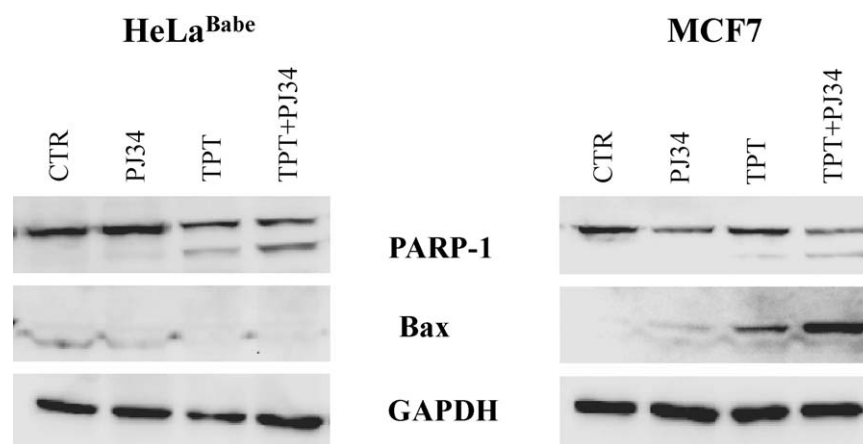


Fig. 9. Western blot analysis of PARP-1 and BAX in HeLa and MCF7 cells. Cells were treated with 10 μ M TPT for 1 h and allowed to recover in fresh medium in the presence or absence of PJ34 for 72 h. GAPDH was used as loading control.

Our data also suggest a synergistic interaction of PARP-1 and PARP-2 with p53 in tumour suppression through their role in DNA damage response and genome integrity surveillance. Another study showed that in MCF7 cells inhibition of endogenous PARP-1 function suppresses the transactivation function of p53 in response to ionizing radiation [28]. We also observed that p53-dependent BAX expression and caspase-dependent PARP-1 proteolysis were sustained by the PARP inhibitor as a result of apoptosis induction.

By the all of such evidences we envisaged a TPT-dependent DNA damage signaling network, involving PARP. Indeed, the DNA damage arising from the trapping of TOP1 was signaled by PARP-1 and -2 and gathered by effectors like p53 and p21. Previous results suggest that p53 causes resistance of cells to TPT [29]. Our findings suggest a PARP modification induced by TPT-dependent DNA damage, while PARP-1 and -2 inactivation switches on p53/p21 pro-apoptotic role.

Indeed, caspase-dependent PARP-1 proteolysis contributes to restoring the apoptotic program in neoplastic cells. Nuclear caspases-mediated PARP-1 cleavage has been described in camptothecin-induced apoptosis as an early event that precedes the release of cytochrome c and AIF, generally thought to activate the chemotherapy-induced apoptosis by DNA-damaging drugs [30].

In conclusion, our findings contribute to the understanding of the molecular events triggered by TOP1 poison-dependent genomic damage and provide a rationale for the development of new approaches to sensitize cancer cells to chemotherapy.

Acknowledgement

This work was supported by funding from the Italian Ministry of Education and Research "Programmi di Ricerca Scientifica di Rilevante Interesse Nazionale" (PRIN 2007–2009).

References

- [1] Pommier Y. Topoisomerase I inhibitors: camptothecins and beyond. *Nat Rev Cancer* 2006;6:789–802.
- [2] Staker BL, Hjerrild K, Feese MD, Behnke CA, Burgin Jr AB, Stewart L. The mechanism of topoisomerase I poisoning by a camptothecin analog. *Proc Natl Acad Sci USA* 2002;99:15387–92.
- [3] Pommier Y, Redon C, Rao VA, Seiler JA, Sordet O, Takemura H, et al. Repair of and checkpoint response to topoisomerase I-mediated DNA damage. *Mutat Res* 2003;532:173–203.
- [4] Takata M, Sasaki MS, Sonoda E, Morrison C, Hashimoto M, Utsumi H, et al. Homologous recombination and non-homologous end-joining pathways of DNA double strand break repair have overlapping roles in the maintenance of chromosomal integrity in vertebrate cells. *EMBO J* 1998;17:5497–508.
- [5] Essers J, van Steeg H, de Wit J, Swagemakers SM, Vermeij M, Hoeijmakers JH, et al. Homologous and non-homologous recombination differentially affect DNA damage repair in mice. *EMBO J* 2000;19:1703–10.
- [6] Arnaudeau C, Lundin C, Helleday T. DNA double-strand breaks associated with replication forks are predominantly repaired by homologous recombination involving an exchange mechanism in mammalian cells. *J Mol Biol* 2001;307:1235–45.
- [7] Burkle A. Poly(ADP-ribosyl)ation. *LANDES Biosci* 2005.
- [8] Schreiber V, Dantzer F, Ame JC, de Murcia G. Poly(ADP-ribose): novel function for an old molecule. *Nat Rev Mol Cell Biol* 2006;7:517–28.
- [9] Scovassi AI, Poirier GG. Poly(ADP-ribosyl)ation and apoptosis. *Mol Cell Biochem* 1999;199:125–37.
- [10] Malanga M, Pleschke JM, Kleczkowska HE, Althaus FR. Poly(ADP-ribose) binds to specific domains of p53 and alters its DNA binding functions. *J Biol Chem* 1998;273(19):11839–43.
- [11] Malanga M, Althaus FR. The role of poly(ADP-ribose) in the DNA damage signaling network. *Biochem Cell Biol* 2005;83(3):354–64.
- [12] Malanga M, Althaus FR. Poly(ADP-ribose) reactivates stalled DNA topoisomerase I and induces DNA strand break resealing. *J Biol Chem* 2004;279(7):5244–8.
- [13] Smith LM, Willmore E, Austin CA, Curtin NJ. The novel poly(ADP-Ribose) polymerase inhibitor, AG14361, sensitizes cells to topoisomerase I poisons by increasing the persistence of DNA strand breaks. *Clin Cancer Res* 2005;11:8449–57.
- [14] Tentori L, Graziani G. Chemopotentiation by PARP inhibitors in cancer therapy. *Pharmacol Res* 2005;52:25–33.
- [15] Sandhu SK, Yap TA, de Bono JS. Poly(ADP-ribose) polymerase inhibitors in cancer treatment: a clinical perspective. *Eur J Cancer* 2010;46(1):9–20.
- [16] Cimmino G, Pepe S, Laus G, Chianese M, Prece D, Penitente R, Quesada P. Poly(ADPR)polymerase-1 signalling of the DNA damage induced by DNA topoisomerase I poison in D54(p53wt) and U251(p53mut) glioblastoma cell lines. *Pharmacol Res* 2007;55(1):49–56.
- [17] Gambi N, Tramontano F, Quesada P. Poly(ADPR)polymerase inhibition and apoptosis induction in cDDP-treated human carcinoma cell lines. *Biochem Pharmacol* 2008;75(12):2356–63.
- [18] Bryant HE, Schultz N, Thomas HD, Parker KM, Flower D, Lopez E, et al. Specific killing of BRCA2-deficient tumours with inhibitors of poly(ADP-ribose) polymerase. *Nature* 2005;434(7035):913–7.
- [19] Davis PL, Shaiu WL, Scott GL, Iglehart JD, Hsieh TS, Marks JR. Complex response of breast epithelial cell lines to topoisomerase inhibitors. *Anticancer Res J* 1998;18(4C):2919–32.
- [20] Tentori L, Muzi A, Dorio AS, Scarsella M, Leonetti C, Shah GM, et al. Pharmacological inhibition of Poly(ADP-ribose) polymerase (PARP) activity in PARP-1 silenced tumour cells increases chemosensitivity to temozolomide and to a N3-adenine selective methylating. *Agent Curr Cancer Drug Targets* 2010;10(4):368–83.
- [21] Tice RR, Agurell E, Anderson D, Burlinson B, Hartmann A, Kobayashi, et al. Single cell gel/comet assay: guidelines for in vitro and in vivo genetic toxicology testing. *Environ Mol Mutagen* 2000;35:206–21.
- [22] Giansanti V, Donà F, Tillhon M, Scovassi AI. PARP inhibitors: new tools to protect from inflammation. *Biochem Pharmacol* 2010. Apr 22 [Epub ahead of print] PMID: 20417190.
- [23] Rouleau M, Patel A, Hendzel MJ, Kaufmann SH, Poirier GG. PARP inhibition: PARP1 and beyond. *Nat Rev Cancer* 2010;10:293–301.
- [24] Yelamos J, Schreiber V, Dantzer F. Toward specific functions of poly(ADP-ribose) polymerase-2. *Trends Mol Med* 2008;14(4):169–78.
- [25] Hastak K, Alli E, Ford JM. Synergistic chemosensitivity of triple-negative breast cancer cell lines to PARP inhibition, gemcitabine and cisplatin. *Cancer Res* 2010. Aug 26 [Epub ahead of print] PMID: 20798217.
- [26] Feeney GP, Errington RJ, Wiltshire M, Marquez N, Chappell SC, Smith PJ. Tracking the cell cycle origins for escape from topotecan action by breast cancer cells. *Br J Cancer* 2003;88(8):1310–7.

- [27] Tuguri S, Crabbé L, Conti C, Tourrière H, Holtgreve-Grez H, Jauch A, et al. Topoisomerase I suppresses genomic instability by preventing interference between replication and transcription. *Nat Cell Biol* 2009;11(11):1315–24.
- [28] Wieler S, Gagné JP, Vaziri H, Poirier GG, Benchimol S. Poly(ADP-ribose) polymerase-1 is a positive regulator of the p53-mediated G1 arrest response following ionizing radiation. *J Biol Chem* 2003;278:18914–21.
- [29] Tomicic MT, Christmann M, Kaina B. Topotecan-triggered degradation of topoisomerase I is p53-dependent and impacts cell survival. *Cancer Res* 2005;65(19):8920–6.
- [30] Rodriguez-Hernandez A, Brea-Calvo G, Fernandez-Ayala DJM, Cordero M, Navas P, Sanchez-Alcazar JA. Nuclear caspase-3 and caspase-7 activation, and poly(ADP-ribose) polymerase cleavage are early events in camptothecin-induced apoptosis. *Apoptosis* 2006;11:131–9.